

The basic theoretical framework for MHD wave propagation in structured media was developed well in advance of the observational evidence for oscillations. For example, Edwin and Roberts (1982) studied wave propagation in coronal loops modelled as straight magnetic slabs. Straight cylindrical flux tube models were used by Spruit (1981); Edwin and Roberts (1983); Roberts (1983). More recent models have explored other effects, such as the curvature of coronal loops (Van Doorselaere *et al.* 2004; Brady and Arber, 2005; Díaz, 2006; Díaz, Zaqarashvili, and Roberts, 2006; Terradas, Oliver, and Ballester, 2006; Verwichte, Foullon, and Nakariakov, 2006a, b); the non-circularity of their cross-sections (Ruderman, 2003) or the influence of a longitudinally-varying density (Andries *et al.* 2005; Andries, Arregui, and Goossens 2005; Arregui *et al.* 2005; McEwan *et al.* 2006; Dymova and Ruderman 2006). Recent comprehensive reviews on these and other studies can be found in Nakariakov and Verwichte (2005) and Aschwanden (2006).

Among all these studies, surface waves have been the subject of considerable attention. Jain and Roberts (1996) studied the properties of magneto-acoustic surface waves at a single interface, for the case of non-parallel propagation, in the context of f -mode oscillations. In a different context Zhelyazkov, Murawski, and Goossens (1996) considered the propagation of magneto-acoustic surface waves with both non-parallel propagation and a sheared magnetic field. Similar studies of surface waves can be found in Roberts (1981a) and Miles and Roberts (1989). By surface wave we mean a wave with an evanescent tail that propagates on a sharp (discontinuous) interface, although they can also propagate on a smoothly varying interface (see Lee and Roberts, 1986; Hollweg, 1990a, b, 1991; Goossens, 1991, for example). Surface waves are expected to occur in the solar atmosphere at places where physical parameters change abruptly. Their propagation is directional and guided by the interface and their energy is confined to within roughly a wavelength of the surface. Surface waves may also arise in more complex structures than a single interface, such as slabs and flux tubes. However, the existence of surface waves in a zero- β equilibrium requires the presence of propagation in the direction perpendicular to the magnetic field (Roberts, 1991).

In this paper, damped coronal-loop oscillations (Aschwanden *et al.* 1999; Nakariakov *et al.* 1999) are considered. We adopt a line-tied slab model for a coronal loop and study the MHD wave properties, for oblique propagation of waves, by solving the normal-mode problem as well as the time-dependent problem. The non-uniformity of the equilibrium produces the resonant damping of these oscillations (Goossens, Andries, and Arregui, 2006). Although the model adopted in this work is an oversimplification, and is far from being an accurate representation of real coronal loops, the simplicity of the model allows a detailed study of the problem and a comparison with the results in a cylindrical loop model.

The layout of the paper is as follows. In Section 2, the equilibrium configuration and the basic MHD equations governing resonantly-coupled fast and Alfvén modes are presented. Next, in Section 3, the normal mode properties are described. In Section 4, we analyse the temporal evolution of the perturbations after given initial disturbances. Finally, in Section 5, our conclusions are drawn.

2. Equilibrium Configuration, Linear MHD Waves, and Numerical Method

We model the equilibrium magnetic and plasma configuration of a solar coronal loop by means of a one-dimensional, line-tied, over-dense slab in Cartesian geometry. The magnetic field is straight and pointing in the z -direction, $\mathbf{B} = B \hat{\mathbf{e}}_z$. For applications to the solar corona it is a good approximation to consider that the magnetic pressure dominates over the gas pressure. This classic zero plasma- β limit implies that the magnetic field is uniform and that the density $[\rho(x)]$ or Alfvén speed $[v_A(x)]$ profiles can be chosen arbitrarily. The coronal slab is then modelled using a varying equilibrium density profile in the x -direction (see Figure 1), by means of a density enhancement of half-width a centred about $x = 0$. The density inside the slab is constant $[\rho_i]$ and connected to the constant coronal environment, with density ρ_e , by transitional non-uniform layers of thickness l . The explicit expression for the equilibrium density considered is

$$\rho(x) = \begin{cases} \rho_i & 0 \leq x \leq a - \frac{l}{2}, \\ f(x) & a - \frac{l}{2} \leq x \leq a + \frac{l}{2}, \\ \rho_e & x \geq a + \frac{l}{2}, \end{cases} \quad (1)$$

with $\rho(-x) = \rho(x)$. The density profiles at the non-uniform transitional layers have been chosen following Ruderman and Roberts (2002); Van Doorselaere *et al.* (2004) and are given by

$$f(x) = \frac{\rho_i}{2} \left[\left(1 + \frac{\rho_e}{\rho_i} \right) - \left(1 - \frac{\rho_e}{\rho_i} \right) \sin \frac{\pi(x-a)}{l} \right]. \quad (2)$$

We remark that the particular form of the density profile at the non-uniform layers has no importance by itself for the results obtained.

In order to study small-amplitude oscillations of the previous equilibrium, the linear resistive MHD equations with constant magnetic diffusivity $[\eta]$ are considered. The inclusion of dissipative terms in the MHD equations is needed for the computation of resonantly-damped eigenmodes. Resistive dissipation is preferred over viscous dissipation for the simplicity with which it enters into the equations. Both dissipation mechanisms affect the thickness of the dissipation layers and the behaviour of the solutions in those layers, but not the differences in the solutions across the layers, which in turn determine the damping rate of the eigenmodes (Sakurai, Goossens, and Hollweg 1991). As the equilibrium configuration only depends on the x -coordinate, a spatial dependence of the form $\exp^{-i(k_y y + k_z z)}$ is assumed for all perturbed quantities, with k_y and k_z being the perpendicular and parallel wave numbers. The photospheric line-tying effect is then included by selecting the appropriate parallel wavenumber. This leads to the following set of differential equations for the two components of the velocity perturbation $[v_x$ and $v_y]$ and the three components of the perturbed magnetic field $[b_{1x}$, b_{1y} , and $b_{1z}]$

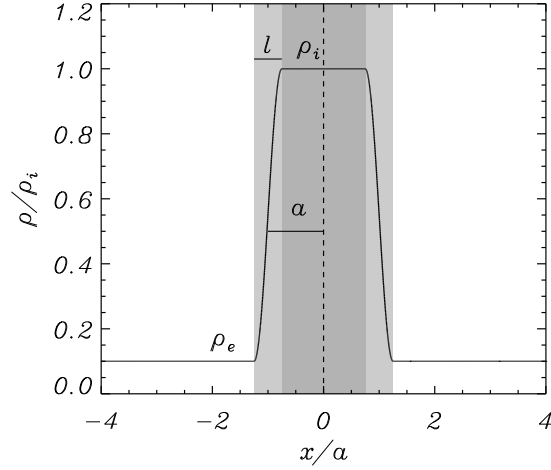


Figure 1. Schematic representation of the density enhancement (shaded region) of half-width a located at $x = 0$ used to model a coronal loop. The internal region with density ρ_i is connected to the external medium, with density ρ_e , by transitional non-uniform layers (light-shaded regions) of thickness l . Non-uniform layers of thickness $l/a = 0.5$ have been considered.

$$\frac{\partial v_x}{\partial t} = \frac{B}{\mu\rho} \left(-ik_z b_{1x} - \frac{\partial b_{1z}}{\partial x} \right), \quad (3)$$

$$\frac{\partial v_y}{\partial t} = \frac{B}{\mu\rho} (-ik_z b_{1y} + ik_y b_{1z}), \quad (4)$$

$$\frac{\partial b_{1x}}{\partial t} = -iBk_z v_x + \eta \left[\frac{\partial^2 b_{1x}}{\partial x^2} - (k_y^2 + k_z^2) b_{1x} \right], \quad (5)$$

$$\frac{\partial b_{1y}}{\partial t} = -iBk_z v_y + \eta \left[\frac{\partial^2 b_{1y}}{\partial x^2} - (k_y^2 + k_z^2) b_{1y} \right], \quad (6)$$

$$\frac{\partial b_{1z}}{\partial t} = -B \left(\frac{\partial v_x}{\partial x} - ik_y v_y \right) + \eta \left[\frac{\partial^2 b_{1z}}{\partial x^2} - (k_y^2 + k_z^2) b_{1z} \right], \quad (7)$$

where μ is the permeability of free space. When $k_y \neq 0$ and $l/a \neq 0$, Equations (3)–(7), describe the oscillatory properties of coupled fast and Alfvén modes. As the plasma- $\beta = 0$, the slow mode is absent and there are no motions parallel to the equilibrium magnetic field, $v_z = 0$. In this paper, solutions to these equations are obtained by performing two kinds of analysis. First the normal modes of oscillation of the system are studied and then the time-dependent evolution of the slab after an initial disturbance is investigated. When only oblique propagation is considered ($k_y \neq 0$), the normal-mode solutions can be obtained by solving an analytical dispersion relation. If, in addition, transitional non-uniform layers are included ($l \neq 0$), the solutions to these equations are, in general, difficult to obtain. For this reason, numerical approximations are obtained using PDE2D (Sewell, 2005), a general-

purpose partial differential equation solver. As for the boundary conditions, in both the normal mode analysis as well as in time-dependent simulations, we impose the vanishing of the perturbed velocity far away from the loop, hence $\mathbf{v} \rightarrow 0$ as $x \rightarrow \pm\infty$.

3. Normal Mode Analysis

We first consider the normal modes of oscillation of our equilibrium configuration. A temporal dependence of the form $e^{i\omega t}$ is assumed for all perturbed quantities in Equations (3)–(7), with $\omega = \omega_R + i\omega_I$ being the complex frequency. These equations form an eigenvalue problem. The solutions for the simplest case, with $k_y = 0$ and $l = 0$, are well-known and described by Edwin and Roberts (1982). They can be classified, according to the parity of their eigenfunctions about $x = 0$, as fast kink and sausage modes. The corresponding dispersion relations are

$$\tanh \kappa_i a = -\frac{\kappa_e}{\kappa_i}, \quad (8)$$

for kink modes (v_x even about $x = 0$) and

$$\coth \kappa_i a = -\frac{\kappa_e}{\kappa_i}, \quad (9)$$

for sausage modes (v_x odd about $x = 0$), where

$$\kappa_e^2 = k_z^2 - \frac{\omega^2}{v_{Ae}^2} \quad \text{and} \quad \kappa_i^2 = k_z^2 - \frac{\omega^2}{v_{Ai}^2}. \quad (10)$$

Here $v_{Ai,e} = B\sqrt{1/\mu\rho_{i,e}}$ are the internal and external Alfvén speeds. Trapped waves have real frequencies whereas modes with complex frequency represent leaky waves. For the modes with the lowest number of internal nodes, the body sausage mode is leaky in the long wavelength limit, $k_z a \ll 1$, while the kink mode is trapped for all wavelengths. All other branches, kink and sausage alike, are leaky in the long-wavelength limit.

The propagation of fast magneto-acoustic waves in a plasma density inhomogeneity with smooth transversal density profiles was considered by Edwin and Roberts (1988) and Nakariakov and Roberts (1995). The latter found that the simple slab profile is a good general guide to the behaviour in a smooth, sharply-structured, profile. Here, a similar smooth transverse density profile is considered and oblique propagation of perturbations included. We will restrict our analysis to trapped modes, whereas for an analysis of the leaky solutions with $k_y = 0$ the reader is referred to Terradas, Oliver, and Ballester (2005).

3.1. Undamped Surface and Body Waves for Oblique Propagation

We first consider the changes of the oscillatory properties of fast modes due to the inclusion of oblique propagation of perturbations. If the slab is connected to the external medium by discontinuities ($l = 0$) Equations (3)–(7) can be combined to give a single ordinary differential equation for the transverse component of the perturbed velocity of the form

$$\frac{d}{dx} \left[\frac{\rho v_A^2 (k_z^2 v_A^2 - \omega^2)}{(k_y^2 + k_z^2) v_A^2 - \omega^2} \frac{dv_x}{dx} \right] - \rho (k_z^2 v_A^2 - \omega^2) v_x = 0. \quad (11)$$

Solutions to this equation can readily be obtained, for ρ and v_A constant, by following the usual procedure of matching different solutions in the internal and external regions (Edwin and Roberts, 1982) and demanding the evanescence of perturbations far away from the slab. This leads to the following dispersion relations

$$\tanh m_i a = -\frac{\kappa_e^2}{\kappa_i^2} \frac{m_i}{m_e}, \quad (12)$$

for kink modes and

$$\coth m_i a = -\frac{\kappa_e^2}{\kappa_i^2} \frac{m_i}{m_e}, \quad (13)$$

for sausage modes, where

$$m_e^2 = \left(k_y^2 + k_z^2 - \frac{\omega^2}{v_{Ae}^2} \right) \quad \text{and} \quad m_i^2 = \left(k_y^2 + k_z^2 - \frac{\omega^2}{v_{Ai}^2} \right). \quad (14)$$

Equations (12) and (13) reduce to Equations (8) and (9) when $k_y = 0$, as expected. An interesting solution of the dispersion relations can be obtained in the limit of quasi-perpendicular propagation, $k_y \gg k_z$, and additionally assuming that $k_y^2 \gg (k_z^2 - \omega^2/v_{Ai}^2)$. Then, the left hand-side of the dispersion relations given by Equations (12) and (13) can be approximated to

$$\left\{ \begin{array}{l} \tanh \\ \coth \end{array} \right\} m_i a \simeq 1. \quad (15)$$

Let us define ω_k as the frequency in this limit. Then, the following expression for the parallel phase speed is obtained

$$\frac{\omega_k}{k_z} \simeq \sqrt{\frac{\rho_i v_{Ai}^2 + \rho_e v_{Ae}^2}{\rho_i + \rho_e}} \equiv c_k, \quad (16)$$

where c_k is the kink speed. This quantity arises also in the description of the kink mode of oscillation of a magnetic flux tube (*e.g.* Spruit, 1981; Ryutova, 1990; Roberts, 1991) and in the propagation of surface waves in the incompressible limit (Roberts, 1981b).

Solutions to Equations (12) and (13) can be found by means of a simple numerical program. In our numerical calculations, we consider fixed values for the density contrast, $\rho_i/\rho_e = 10$, and for the parallel wavenumber, $k_z a = \pi/50$. For the observed transverse kink-mode oscillations, with a wavelength double the length of the loop, this corresponds to a ratio of length to width of $L/2a = 25$, which is a typical value for observed oscillating coronal loops. Figure 2 displays some solutions as a function of the perpendicular wave number. The dispersion relations have two frequencies

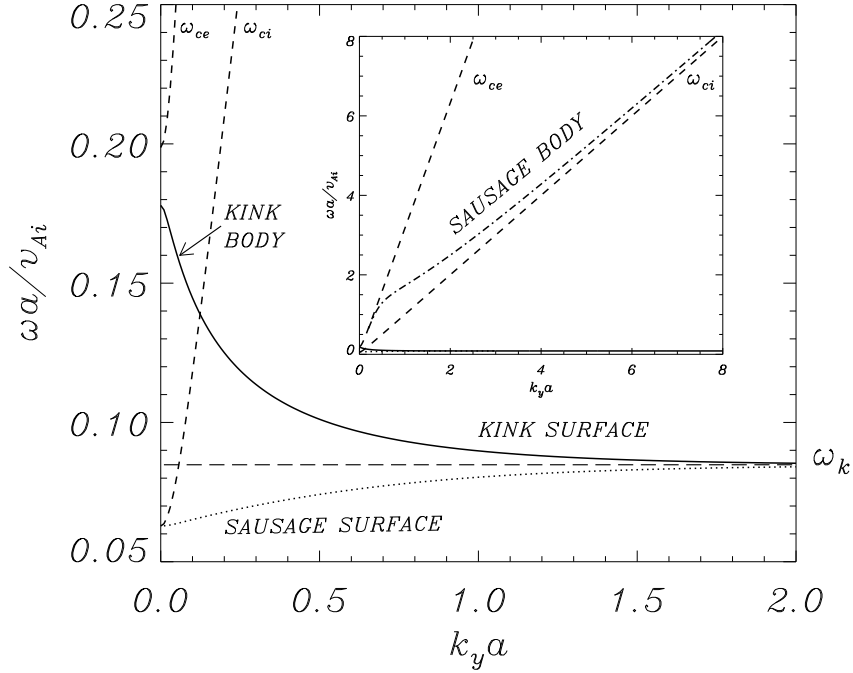


Figure 2. Dispersion diagram calculated from the numerical solution of the dispersion relations, Equations (12) and (13), for a slab model of coronal loop with $k_z a = \pi/50$ and density contrast $\rho_i/\rho_e = 10$. The frequency of the different solutions is displayed as a function of the perpendicular wave number: kink mode (solid), sausage surface mode (dotted) and sausage body (dash-dotted). The horizontal long-dashed line indicates the frequency ω_k , given by Equation (16), to which both kink and sausage surface waves approach for large k_y . The inset plot displays a broader view of the solutions in order to show the behaviour of the sausage body solution. The dashed lines represent the internal and external cut-off frequencies, $\omega_{ci} = \sqrt{k_y^2 + k_z^2} v_{Ai}$ and $\omega_{ce} = \sqrt{k_y^2 + k_z^2} v_{Ae}$ respectively. For large k_y , the sausage body mode approaches asymptotically ω_{ci} never crossing below its value and the kink and sausage surface solutions go to the kink frequency given by Equation (16).

at which the characteristics of wave motions vary. Modes with a frequency above the external cut-off frequency $\left[\omega_{ce} = v_{Ae} \sqrt{k_y^2 + k_z^2} \right]$ are leaky. The internal cut-off frequency $\left[\omega_{ci} = v_{Ai} \sqrt{k_y^2 + k_z^2} \right]$ also plays an important role, since depending on whether the frequency of the eigenmode is above or below this cut-off we have a body-like or a surface-like mode.

The kink-mode solution has a decreasing frequency with respect to k_y . For small values of k_y its frequency is above the internal cut-off frequency ($m_i^2 < 0$, in Equation (12)) and the mode is a body wave. Beyond a given value of k_y ($k_y a \sim 0.15$ in Figure 2), however, the frequency crosses the internal cut-off frequency ($m_i^2 > 0$) and the mode becomes a surface solution. In addition, as soon as $k_y \neq 0$, there is also a solution with frequency near the internal cut-off frequency. This solution is always below the internal cut-off frequency and, therefore, corresponds to a surface wave.

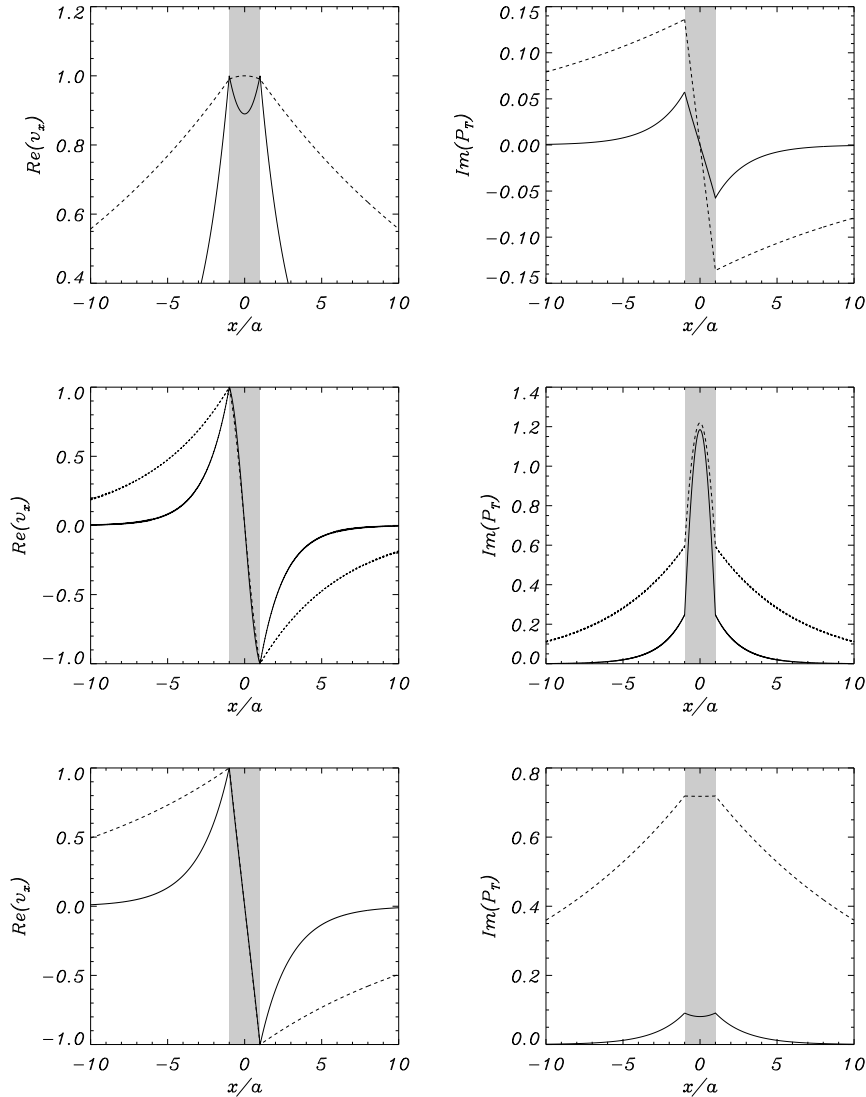


Figure 3. Real part of the transverse velocity component $[v_x]$ and imaginary part of the perturbed total pressure $[P_T]$ for the fundamental kink mode (*top panels*), the sausage body mode (*middle panels*) and the sausage surface mode (*bottom panels*) for an equilibrium configuration with $k_z a = \pi/50$, $\rho_i/\rho_e = 10$ and two values of the perpendicular wave number: $k_y a = 0.0$ (dotted lines) and $k_y a = 0.5$ (solid lines) for the top and bottom panels and $k_y a = 0.2$ (dotted lines) and $k_y a = 0.5$ (solid lines) for the middle panel. Note that the character of the eigenfunction for the kink mode changes from body-like to surface-like and that for $k_y a = 0.5$ the sausage body and surface mode solutions have an almost identical v_x . In all figures, the shaded region represents the density enhancement.

For this solution v_x has odd parity with respect to $x = 0$ and so is a sausage surface wave. For increasing k_y the sausage surface mode approaches the kink mode solution

and for large k_y both asymptotically tend to the frequency given by Equation (16). Therefore, for almost perpendicular propagation there are two surface modes corresponding to the two parities allowed by the symmetry of the problem. Contrary to the case $k_y = 0$, the mode with lowest frequency is sausage and not kink. The inset plot in Figure 2 displays a broader view of the solutions. The sausage body solution is leaky for small values of k_y , but it becomes non-leaky and its frequency is that of the external cut-off frequency near $k_y a = 0.2$. Then, for increasing k_y its frequency increases. In contrast to the kink-mode solution the frequency of the sausage body mode never crosses below the internal cut-off frequency, but approaches asymptotically its value for increasing k_y . The reason for this behaviour is that there is already a solution with odd parity with respect to $x = 0$ below the internal cut-off frequency.

We obtain further information on the properties of the normal modes from the spatial distribution of the eigenfunctions. Figure 3 shows the perturbed transverse velocity $[v_x]$ and the perturbed magnetic pressure $[P_T]$ obtained from b_{1z} , for two different values of the perpendicular wave number and for the fundamental kink eigenmode, the sausage body mode and the sausage surface mode. Significant changes of the properties of eigenfunctions are clearly visible as the value of the perpendicular wave number is increased. For $k_y = 0$, the kink mode has its characteristic behaviour with a maximum of v_x at the internal part of the slab, while v_x decreases exponentially for increasing distance from the loop. On the other hand, the total pressure perturbation for this mode has the usual antisymmetric profile with a zero value at the centre of the slab and maxima at its edges. When oblique propagation is included ($k_y \neq 0$), there is an increased confinement of the eigenfunctions, compared with non-oblique propagation. This result, also found by Díaz, Oliver, and Ballester (2003) in the context of prominence fibril oscillations, can be seen in terms of a sharper drop-off rate of the mode in the external medium. The solutions for $k_y a \neq 0$ over-plotted in Figure 3 correspond to a value for which the kink solution is already below the internal cut-off frequency and show significant changes with respect to the $k_y = 0$ case. The kink mode becomes a surface-like mode and motions are more confined to the edges of the slab. Further increase of k_y produces a more marked confinement and a lower amplitude inside the slab. The middle and bottom panels of Figure 3 show the eigenfunctions for the body and surface sausage modes. The most important property is the similarity in the transverse component of the velocity for both solutions when k_y is sufficiently large and also that the motions are very confined to the edges of the slab. The magnetic-pressure perturbation distribution peaks at the centre of the slab for the body solution, while it is maximum at the edges in the case of the surface solution. Finally, oblique propagation of waves affects the magnitude of the total pressure perturbation of the surface sausage mode, but not very much that of the body sausage mode inside the density enhancement.

3.2. Damping of Oscillations by Resonant Absorption

In this section the most general equilibrium configuration considered in this work is taken. The uniform internal density of the slab is now connected to the external (coronal) medium by means of non-uniform transitional layers. This produces damping by resonant coupling of fast modes to Alfvén waves (Hollweg and Yang, 1988; Goossens, Andries, and Arregui, 2006). In order to solve Equations (3)–(7), in this case we have to resort to numerical techniques and the numerical code PDE2D is

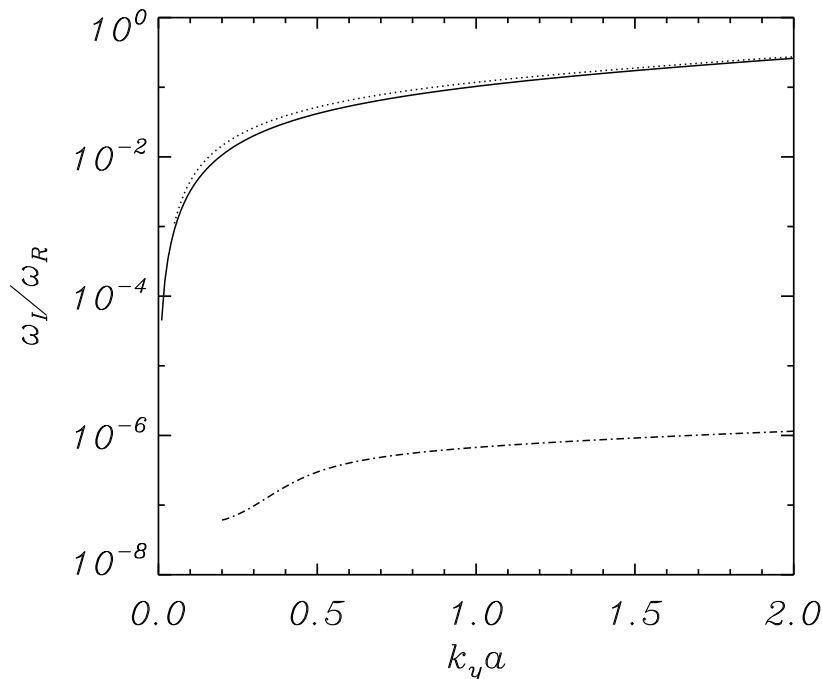


Figure 4. Damping rate for the resonantly-damped fast kink surface mode (solid line), sausage surface mode (dotted line) and sausage body mode (dash-dotted line) as a function of the perpendicular wave number in a coronal slab model with $k_z a = \pi/50$, $\rho_i/\rho_e = 10$ and non-uniform transitional layers with thickness $l/a = 0.5$. A value for the magnetic Reynolds number of $R_m/v_{A_i} a = 10^7$ has been used in the computation of the solutions in a non-uniform grid with $N_x = 10\,000$ points in the range $-50 \leq x/a \leq 50$.

used. The code uses finite elements and allows the use of non-uniformly distributed grids, which is needed in order to better resolve the large gradients that arise in the vicinity of the resonant layers and has been used successfully, in a similar problem, by Terradas, Oliver, and Ballester (2006). For the normal-mode analysis, a small but finite value of resistivity has to be provided when computing the damping of oscillations. Resistivity has to be small enough for the imaginary part of the frequency to be independent of resistivity (Poedts and Kerner, 1991). This condition has been checked to a high accuracy for the solutions presented in this paper and a value for the magnetic Reynolds number, $R_m/v_{A_i} a$, between 10^6 and 10^8 has been sufficient.

The same parameter values for the equilibrium configurations are considered. Non-uniform transitional layers of thickness $l/a = 0.5$ have been considered and we have computed the real and imaginary parts of the frequency for the kink mode and the sausage surface and body modes, for varying perpendicular wave number. The results are displayed in Figure 4. When we increase k_y , the damping rates of the kink mode and the sausage surface mode increase. Both damping rates are very similar, despite the different symmetry of the motions. The damping rate corresponding to

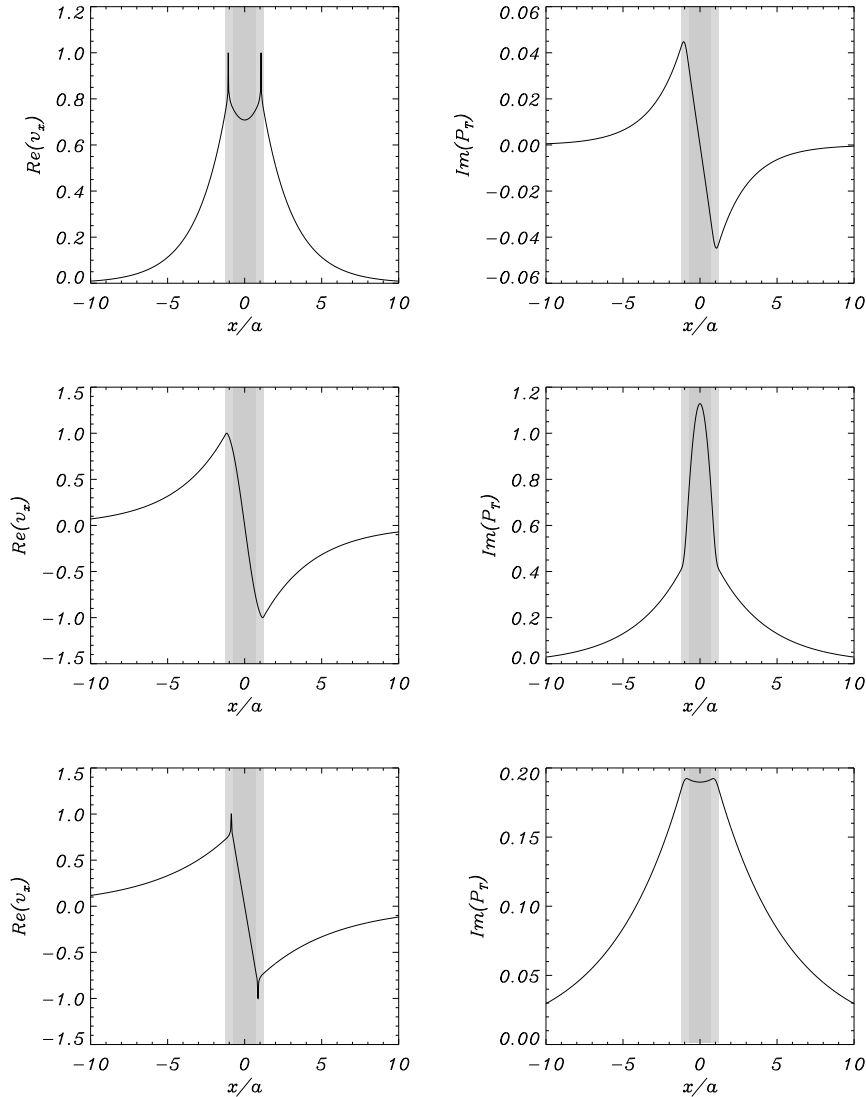


Figure 5. Real part of the transverse velocity component, v_x and imaginary part of the perturbed total pressure for the fundamental kink mode (*top panels*), the sausage body mode (*middle panels*) and the sausage surface mode (*bottom panels*) for an equilibrium configuration with $k_z a = \pi/50$, $\rho_i/\rho_e = 10$, $k_y a = 0.5$ and non-uniform transitional layers with thickness $l/a = 0.5$. A value for the magnetic Reynolds number of $R_m/v_{A1}a = 10^7$ has been used in the computation of the solutions in a non-uniform grid with $N_x = 10\,000$ points in the range $-50 \leq x/a \leq 50$. In all figures, the shaded region represents the density enhancement and the light-shaded regions the non-uniform layers.

the sausage body mode is roughly four to five orders of magnitude smaller than the one corresponding to the two surface modes and practically of the order of the used magnetic diffusivity. The reason for the absence of resonant damping in the

case of the sausage body solution is that its frequency, for the case of $k_z a$ small, lies outside the Alfvén continua produced by the presence of the non-uniform layers defined by the interval $[V_{Ai}k_z, V_{Ae}k_z]$ (see Figure 2). In conclusion, surface-like kink and sausage oscillations are likely to be damped out rapidly, by resonant conversion of energy, while body-like sausage modes are unaffected by resonant absorption.

Figure 5 displays example eigenfunctions obtained from the computed resonantly damped eigensolutions. All three modes under consideration, the sausage surface and body modes and the kink mode, are displayed. The spatial distribution of eigenfunctions is rather similar to the ones shown in Figure 3, but now peaks at the non-uniform transitional layers are clearly visible at the perturbed transverse velocity of the kink mode and the sausage surface mode, while they are absent in the case of the sausage body mode. These peaks are an indication of resonant coupling to Alfvén waves at the non-uniform layers. Aside from these peaks, the spatial distribution of the magnetic pressure perturbation has extrema at the resonant layers in the case of the kink mode and the sausage surface mode, while it is maximum at the centre of the slab in the case of the sausage body mode. The total pressure perturbation has no extrema at the resonant layers in the case of the sausage body solution. The behaviour of the eigenfunctions at the resonant layers and the fundamental conservation laws that govern the resonant couplings were studied by Sakurai, Goossens, and Hollweg (1991) in ideal MHD and by Goossens, Ruderman, and Hollweg (1995) in dissipative MHD. These authors find that the derivative of the total pressure perturbation is zero at the resonant positions. This behaviour is retrieved in the pressure perturbation for our damped surface-like solutions, but not in the case of the sausage body solutions, for which resonant couplings are absent.

4. Time-Dependent Analysis

The normal-mode analysis has provided us with information on the spatial scales of the eigenmodes of the system and their relation to the frequency of the eigenmodes. The issue of the excitation of oscillations is now considered. Observed transverse coronal-loop oscillations have been found to be mainly produced by impulsive events, such as filament eruptions or flare-generated blast waves. Previous studies have considered the temporal evolution of initial pulses in a magnetic slab. For instance, Murawski and Roberts (1993a, b) studied the energy leakage associated with the propagation of sausage and kink waves in smoothed slabs and the temporal evolution of impulsively-generated linear waves, respectively. Murawski, Aschwanden, and Smith (1998) studied the different propagation phases (periodic, quasi-periodic, and decay) of impulsively-generated waves in solar coronal loops, with arbitrary plasma- β . More recently, Nakariakov, Pascoe, and Arber (2005) have demonstrated the possibility of remote diagnostics of the steepness of the transverse density profile and the density contrast in coronal loops, with impulsively-generated, short-period, fast magneto-acoustic wave trains. From a theoretical point of view, it is of interest to study the distribution of the energy of an initial perturbation among the different normal modes of the system, as well as the study of the conditions under which one or other type of mode of oscillation is excited in the system. The amount of energy that is deposited in the trapped fast mode oscillation, for different initial excitations, has been studied by Terradas, Andries, and Goossens (2007), for a cylindrical magnetic tube. These authors find that the amount of energy deposited in the loop depends

on the shape and distance of the initial perturbation. In this paper, we are interested in the conversion of energy from fast modes to Alfvén modes and the comparison of the oscillatory properties of the excited disturbances, such as the period and the damping, with the results of the normal mode analysis. For this reason, we show results of numerical simulations of the linearised MHD equations performed with initial disturbances that deposit a considerable amount of energy in the loop. As the normal modes studied in Section 3 are characterised by their symmetry around $x = 0$, it is likely that an initial disturbance with a given symmetry will excite one or the other types of mode. For this reason we have performed numerical simulations with two different types of initial disturbances, namely v_x symmetric and antisymmetric with respect to $x = 0$.

To solve Equations (3)–(7) numerically we have used the time-dependent version of the PDE2D code. Also, η is now set to zero. The code uses a second-order Crank-Nicholson method with adaptive time-step control. Since we are considering a finite domain, reflections at the domain boundaries may affect the dynamics of the simulated loop. We have solved this problem by locating the edges of the numerical domain far enough from the loop. Given that the size of the domain is much larger than the loop thickness, we have used a non-uniform grid with 10 000 grid points in the full domain, one fifth of them located inside the loop and another fifth in each inhomogeneous layer.

4.1. Symmetric Excitation

We first consider an initial disturbance on the transverse velocity component with a Gaussian of the form

$$v_x(x, t = 0) = v_{x0} \left\{ \exp \left[- \left(\frac{x - x_0}{w} \right)^2 \right] \right\}, \quad (17)$$

where v_{x0} is the amplitude of the perturbation, x_0 the position of the Gaussian centre and w its width at half-height. This form of excitation aims to simulate the transverse disturbance generated by a flare or filament eruption. Since the numerical computations apply to the linear regime, the particular value of v_{x0} is not relevant and has been set to v_{Ai} .

In order to compare our results with the properties of the eigensolutions described in Section 3, we have considered a slab model of half-width a , density contrast $\rho_i/\rho_e = 10$, and $k_z a = \pi/50$. For the perpendicular wave number and the non-uniform transitional layers thickness we take values of $k_y a = 0.5$ and $l/a = 0.5$. The system is then disturbed with a perturbation given by Equation (17) with $x_0 = 0$ and $w = 2a$. The results of the simulation are shown in Figure 6, where the spatial distribution of the transverse velocity component is plotted at different times. The initial perturbation produces travelling disturbances to the left and right of its initial location and these disturbances exhibit some dispersion as they propagate. After a short time it is seen that the distribution of energy has a maximum at the centre of the system, with the amplitude decreasing as we move away from the edges of the slab. This indicates that the fundamental kink eigenmode may have been excited. The inset plot in the last shown frame supports this idea, since the structure of v_x is almost identical to that of the normal mode, shown in Figure 5. In Figure 7 (left) the velocity at $x = 0$ is plotted. The signal at this position clearly shows a damped

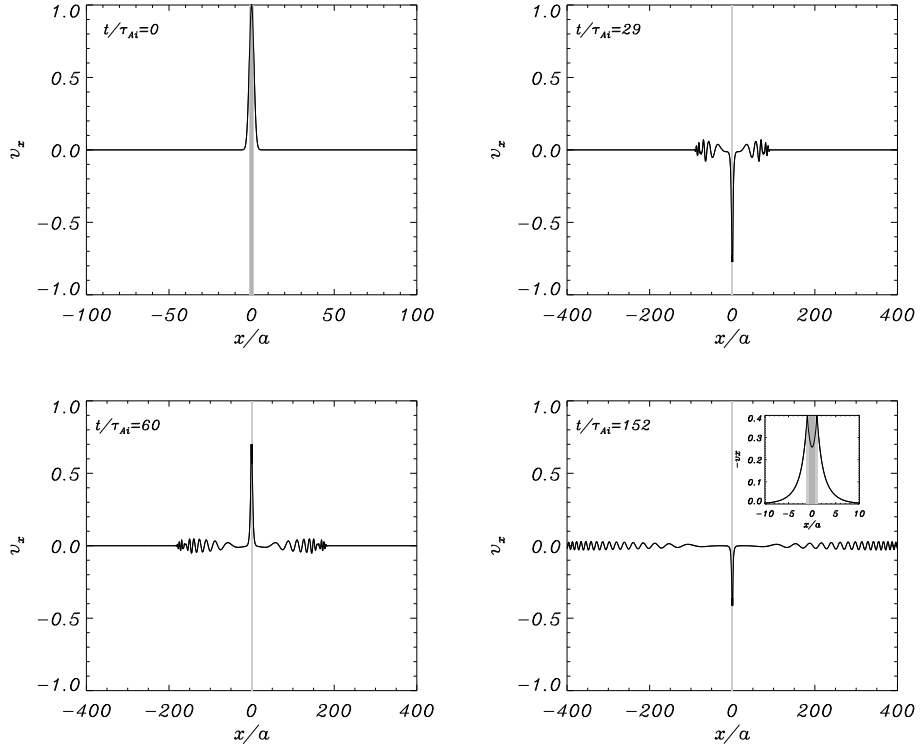


Figure 6. Transverse velocity component, v_x , at different times (in units of the internal Alfvén transit time, $\tau_{Ai} = a/v_{Ai}$) for a symmetric disturbance given by Equation (17), with $x_0 = 0$, $w = 2a$ and $a = 1$. The inset plot in the lower-right frame displays a detailed view of the transverse velocity component of the excited kink mode in order to compare it with the eigenmode computation shown in Figure 5. The grey-shaded regions represent the loop.

oscillatory behaviour. This damping is due to the resonant coupling and conversion of energy to Alfvénic motions. We have performed a periodogram (Figure 7, right) and found that the dominant period agrees very well with the period of the fundamental kink eigenmode obtained in Section 3. The extrema of the signal are then fitted to an exponential of the form $A e^{-\tau_d/t}$. The fitted function is also shown in Figure 7 (left). From the periodogram and the exponential fit we find that the dominant period and damping time agree very well with the oscillatory properties of the kink eigenfunction, which leads to the conclusion that the resonantly damped fundamental kink mode has been excited. Therefore, a symmetric excitation is likely to excite the fundamental kink mode of oscillation of the system.

4.2. Antisymmetric Excitation

Next, we consider the excitation of the slab with an odd perturbation of the form

$$v_x(x, t = 0) = v_{x0} \left\{ \exp \left[- \left(\frac{x - x_0}{w} \right)^2 \right] - \exp \left[- \left(\frac{x + x_0}{w} \right)^2 \right] \right\}, \quad (18)$$

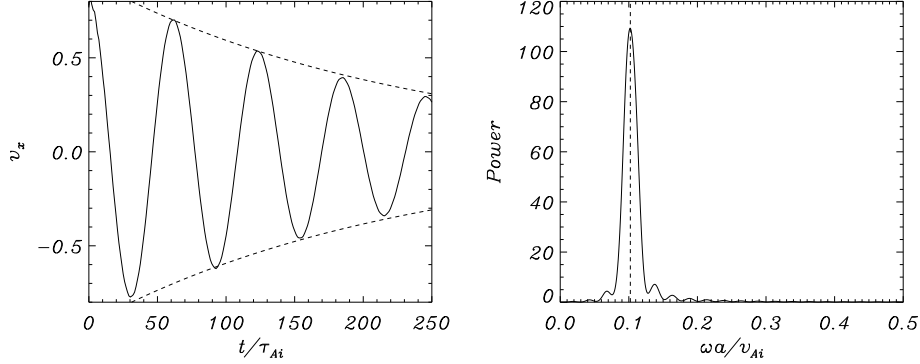


Figure 7. *Left panel:* Transverse velocity $[v_x]$ at the slab centre $[x = 0]$ as a function of time for the simulation shown in Figure 6. After a very short transient phase the loop reaches a stationary state, oscillating at the frequency predicted by the normal mode analysis. The oscillation is damped due to resonant absorption. *Right panel:* Periodogram of the signal, that peaks at $\omega a/v_{Ai} = 0.1018$, in good agreement with the normal mode result, $\omega_{Ra}/v_{Ai} = 0.1022$ (dashed-line). An exponential fit of the signal for v_x gives a damping time $\tau_d/\tau_{Ai} = 225.5$, that corresponds to an imaginary part of the frequency $\omega_I a/v_{Ai} = 4.43 \times 10^{-3}$, in good agreement with the normal mode result, $\omega_{Ia}/v_{Ai} = 4.38 \times 10^{-3}$. Since both the peak power and the damping time agree with the normal-mode results, there is a clear evidence that the fundamental fast kink body mode has been excited.

where v_{x0} , x_0 , and w have the same meaning as before. The system is now disturbed with a perturbation given by Equation (18) with $x_0 = a$ and $w = 2a$. As the surface sausage mode is highly confined to the loop edges, short spatial scales are involved and these scales have to be introduced either through the width of the disturbance or through the value of k_y . The first option complicates the numerical computations, so a value $k_y a = 1.4$ has now been taken. The numerical solutions at different times (Figure 8) show again that the induced disturbances propagate away from the slab and contain different wavelengths due to the dispersive nature of fast waves. After some time, the shape of the velocity around the slab approaches the form of the sausage surface fast wave described in Section 3. In contrast to the kink case, the velocity distribution in the slab is now more complex, since more than one oscillatory mode seems to be present in the signal (see, for example, the inset in the last shown frame). The consequence of this can clearly be seen in Figure 9 (left) where the signal at $x/a = 1$ is shown. The presence of two linearly superposed oscillations is apparent. A short period oscillation is modulated in amplitude with a large period oscillation. The signal is again damped in time. The computation of the dominant periods of the signal gives the result displayed in Figure 9 (right). There are two peaks whose frequencies are in perfect agreement with the frequencies of the sausage surface and body modes, obtained from the normal mode analysis. The power for the body sausage mode is larger, although this may change depending on the spatial scales involved. The damping time of the signal, obtained with a similar exponential fit as in the previous case, does not correspond to any of the two eigenmodes, since the two are present at the same time, but is close to the damping of the sausage surface mode. Therefore, we can conclude that an antisymmetric disturbance located

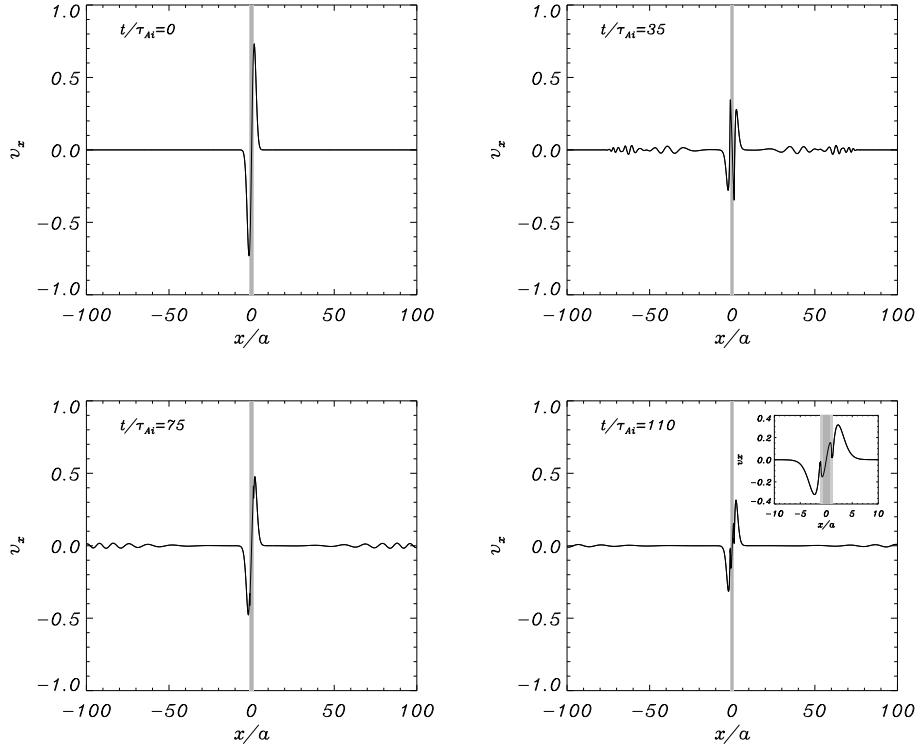


Figure 8. Transverse velocity component [v_x] at different times (in units of the internal Alfvén transit time, $\tau_{Ai} = a/v_{Ai}$), for an antisymmetric disturbance given by Equation (18), with $x_0 = a$, $w = 2a$, and $a = 1$. The inset plot in the lower-right frame displays a detailed view of the transverse velocity component of the excited sausage modes in order to compare it with the eigenmode computations shown in Figure 5. The grey-shaded regions represent the loop.

at the edges of the slab induces the excitation of both types of sausage modes. The reason is that the surface and body sausage modes, although having very different frequencies, have very similar eigenfunctions, when k_y is sufficiently large.

5. Summary and Conclusions

We have studied the oscillatory properties of surface and body MHD eigenmodes of a solar coronal loop including oblique propagation of perturbations. For simplicity, a Cartesian slab model has been considered and both the eigenvalue problem as well as the time-dependent problem have been solved.

The inclusion of oblique propagation of perturbations produces some important effects on the properties of eigenmodes. The resulting dispersion curves for non-zero perpendicular propagation show the existence of a sausage surface mode in addition to the usual fast body kink and sausage solutions, even if a zero-plasma- β has been considered. This mode, not present if $k_y = 0$, has the lowest frequency and this frequency is always below the internal cut-off frequency. For small values of k_y , in

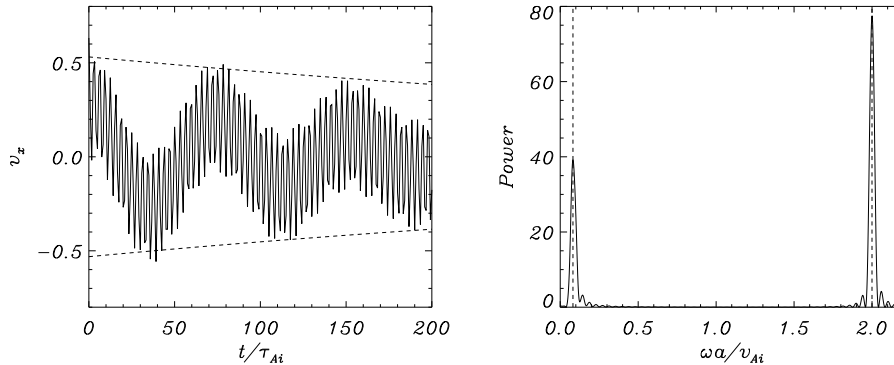


Figure 9. *Left panel:* Transverse velocity [v_x] at the slab edge [$x = a$] as a function of time for the simulation shown in Figure 8. After a very short transient phase the loop oscillates with a linear superposition of two frequencies. The signal is damped due to resonant absorption. A fit of the signal for v_x gives a damping time $\tau_d/\tau_{Ai} = 621.6$, that corresponds to an imaginary part of the frequency $\omega_{I1}a/v_{Ai} = 1.6 \times 10^{-3}$. *Right panel:* Periodogram of the signal that peaks at $\omega_1 a/v_{Ai} = 0.0817$ and $\omega_2 a/v_{Ai} = 1.9998$. The dashed lines represent the frequencies obtained with the normal mode analysis; $\omega_R a/v_{Ai} = 0.0778$ for the sausage surface mode and $\omega_B a/v_{Ai} = 2.0087$ for the sausage body mode. As the damping time of the motion is a linear combination of the damping of the two modes the fitted damping is in between the imaginary parts of the frequency for the sausage surface mode ($\omega_{I1}a/v_{Ai} = 1.35 \times 10^{-2}$) and the sausage body mode ($\omega_{I2}a/v_{Ai} = 1.74 \times 10^{-6}$), for this case. Since the power peaks agree with the normal mode results there is a clear evidence that both the surface and body sausage modes have been excited.

the long-wave limit, the kink eigenmode is a body wave with the usual distribution of the velocity perturbation with a maximum at the centre and an evanescent behaviour outside the slab. The sausage surface mode has a velocity perturbation which is more confined to the edges of the slab with a short penetration depth into the coronal surroundings. When the value of the perpendicular wave number is increased, a marked decrease of the oscillation frequency is produced in the case of the kink mode. The spatial structure of the eigenfunction of this mode becomes much more confined to the slab. This leads to a change in the character of the kink mode which changes from body-like to surface-like. For large values of k_y , both surface modes (kink and sausage) approach the kink speed limit, that corresponds to surface waves in a magnetic interface in the incompressible limit or to the kink eigenoscillations of a cylindrical flux tube in the long wavelength limit. As for the sausage surface mode, there is no appreciable change in its eigenfunction with k_y and only a slight increase on the frequency is produced. The sausage body mode, which is leaky in the long-wavelength limit, becomes trapped when, for a give value of k_y , its frequency equals the external cut-off frequency, ω_{ci} . This is due to the modification of the external cut-off frequency produced by the inclusion of oblique propagation. The internal cut-off frequency is also modified by oblique propagation, but the frequency of the sausage body mode is always above this cut-off frequency, due to the existence of a surface mode with the same symmetry below that cut-off. The eigenfunctions for both sausage solutions have a marked resemblance and this has important consequences on the excitation of these modes. When the density is allowed to vary smoothly between

the constant internal and the constant external values, surface-like eigenmodes are damped by resonant conversion of energy. Both surface modes have a similar damping rate, while the sausage body mode is unaffected by resonant absorption.

In the second part of the paper we have studied the time-dependent behaviour of our line-tied slab model for a coronal loop under different kinds of excitations. The temporal evolution and damping by resonant conversion of wave energy of kink- and sausage-type excitations has been studied for a typical coronal loop. The eigenmodes described in the first part of the paper can be easily excited. A symmetric disturbance located at the centre of the slab excites the fundamental symmetric kink mode. Depending on the value of k_y , the excited mode would have body or surface wave properties. The period of the signal and its damping time agree with the result obtained with the normal mode analysis. The velocity distribution of the stationary phase coincides with the spatial distribution of the eigenfunction. Interestingly, an antisymmetric initial disturbance with peaks at the edges of the slab excites both the surface and the body sausage modes and a linear superposition of perturbations is obtained, with the sausage body oscillation amplitude being modulated by the presence of the sausage surface mode. This can be explained in terms of the involved eigenfunctions since oblique propagation confines the spatial distribution of the body sausage mode and makes it very similar to that of the sausage surface mode.

In this work, a magnetic slab has been used to model a coronal loop. Some of the results found in slab geometry cannot be translated to cylindrical geometry. For instance, the sausage surface mode described in this paper is not present in cylindrical geometry. Also, the sausage mode of oscillation of a cylinder corresponds to an azimuthal wave number $m = 0$, thus this mode cannot resonantly couple to Alfvén modes. Slabs are known to be poor wave-guides, when compared to cylinders. However, our results indicate that the inclusion of oblique propagation produces a sharper drop-off rate of the kink eigenfunction in the external medium and a frequency that is a good approximation to the kink-mode frequency in a slender flux tube.

Acknowledgements We thank the referee, Dr. Erwin Verwichte, for constructive and valuable comments that have benefited this paper. The authors acknowledge the Spanish Ministerio de Educación y Ciencia for the funding provided under project AYA2006-07637 and the Conselleria d'Economia, Hisenda i Innovació of the Government of the Balearic Islands for the funding provided under grants PRIB-2004-10145 and PCTIB2005GC3-03. J. Terradas acknowledges the Spanish Ministerio de Educación y Ciencia for the funding provided under a Juan de la Cierva fellowship.

References

- Andries, J., Arregui, I., Goossens, M.: 2005, *Astrophys. J.* **624**, L57.
 Andries, J., Goossens, M., Hollweg, J.V., Arregui, I., Van Doorselaere, T.: 2005, *Astron. Astrophys.* **430**, 1109.
 Arregui, I., Van Doorselaere, T., Andries, J., Goossens, M., Kimpe, D.: 2005, *Astron. Astrophys.* **441**, 361.
 Arregui, I., Andries, J., Van Doorselaere, T., Goossens, M., Poedts, S.: 2007b, *Astron. Astrophys.* **463**, 333.
 Aschwanden, M.J.: 2006, *Roy. Soc. London Phil. Trans. Ser. A* **364**, 417.
 Aschwanden, M.J., De Pontieu, B., Schrijver, C.J., Title, A.M.: 2002, *Solar Phys.* **206**, 99.
 Aschwanden, M.J., Fletcher, L., Schrijver, C.J., Alexander, D.: 1999, *Astrophys. J.* **520**, 880.

- Aschwanden, M.J., Nightingale, R.W., Andries, J., Goossens, M., Van Doorselaere, T.: 2003, *Astrophys. J.* **598**, 1375.
- Brady, C.S., Arber, T.D.: 2005, *Astron. Astrophys.* **438**, 733.
- Díaz, A.J.: 2006, *Astron. Astrophys.* **456**, 737.
- Díaz, A.J., Oliver, R., Ballester, J.L.: 2003, *Astron. Astrophys.* **402**, 781.
- Díaz, A.J., Zaqarashvili, T.V., Roberts, B.: 2006, *Astron. Astrophys.* **455**, 709.
- Dymova, M.V., Ruderman, M.S.: 2006, *Astron. Astrophys.* **457**, 1059.
- Edwin, P.M., Roberts, B.: 1982, *Solar Phys.* **79**, 239.
- Edwin, P.M., Roberts, B.: 1983, *Solar Phys.* **88**, 179.
- Edwin, P.M., Roberts, B.: 1988, *Astron. Astrophys.* **192**, 343.
- Goossens, M.: 1991 In Ulmschneider, P., Priest E.R., Rosner, R. (eds.), *Mechanisms of Chromospheric and Coronal Heating*, Springer-Verlag, Berlin, 480.
- Goossens, M., Andries, J., Arregui, I.: 2006, *Roy. Soc. London Phil. Trans. Ser. A* **364**, 433.
- Goossens, M., Andries, J., Aschwanden, M.J.: 2002, *Astron. Astrophys.* **394**, L39.
- Goossens, M., Ruderman, M.S., Hollweg, J.V.: 1995, *Solar Phys.* **157**, 75.
- Hollweg, J.V., Yang, G.: 1988, *J. Geophys. Res.* **93**, 5423.
- Hollweg, J.V.: 1990a, *Comp. Phys. Reports* **12**, 205.
- Hollweg, J.V.: 1990b, In Russel, C.T., Priest, E.R., Lee, L.C. (eds.), *Physics of Magnetic Flux Ropes*, (Washington, AGU), Geophys. Mono. 58, 123.
- Hollweg, J.V.: 1991 In Ulmschneider, P., Priest E.R., Rosner, R. (eds.), *Mechanisms of Chromospheric and Coronal Heating*, Springer-Verlag, Berlin, 423.
- Jain, R., Roberts, B.: 1994, *Astron. Astrophys.* **286**, 243.
- Lee, M.A., Roberts, B.: 1986, *Astrophys. J.* **301**, 430.
- McEwan, M.P., Donnelly, G.R., Díaz, A.J., Roberts, B.: 2006, *Astron. Astrophys.* **460**, 893.
- Miles, A.J., Roberts, B.: 1989, *Solar Phys.* **119**, 257.
- Murawski, K., Roberts, B.: 1993a, *Solar Phys.* **143**, 89.
- Murawski, K., Roberts, B.: 1993b, *Solar Phys.* **144**, 101.
- Murawski, K., Aschwanden, M.J., Smith, J.M.: 1998, *Solar Phys.* **179**, 313.
- Nakariakov, V.M., Ofman, L.: 2001, *Astron. Astrophys.* **372**, L53.
- Nakariakov, V.M., Roberts, B.: 1995, *Solar Phys.* **159**, 399.
- Nakariakov, V.M., Verwichte, E.: 2005, *Living Rev. Solar Phys.* **2**, 3.
<http://solarphysics.livingreviews.org>
- Nakariakov, V.M., Pascoe, D.J., Arber, T.D.: 2005, *Space Sci Rev.* **121**, 115.
- Nakariakov, V.M., Ofman, L., DeLuca, E.E., Roberts, B., Davila, J.M.: 1999, *Science* **285**, 862.
- Poedts, S., Kerner, W.: 1991, *Phys. Rev. Lett.* **66**, 2871.
- Roberts, B.: 1981a, *Solar Phys.* **69**, 27.
- Roberts, B.: 1981b, *Solar Phys.* **69**, 39.
- Roberts, B.: 1983, *Solar Phys.* **87**, 77.
- Roberts, B.: 1991, In Ulmschneider, P., Priest E.R., Rosner, R. (eds.), *Mechanisms of Chromospheric and Coronal Heating*, Springer-Verlag, Berlin, 494.
- Roberts, B., Edwin, P.M., Benz, A.O.: 1984, *Astrophys. J.* **279**, 857.
- Ruderman, M.S.: 2003, *Astron. Astrophys.* **409**, 287.
- Ruderman, M.S. and Roberts, B.: 2002, *Astrophys. J.* **577**, 475.
- Ryutova, M. P.: 1990, In Stenflo, J.O. (ed.), *Solar Photosphere: Structure, Convection and Magnetic Fields*, (Reidel, Dordrecht), IAU Symp. 138, 229.
- Sakurai, T., Goossens, M., Hollweg, J.V.: 1991, *Solar Phys.* **133**, 227.
- Sewell, G.: 2005, *The Numerical Solution of Ordinary and Partial Differential Equations*, John Wiley & Sons, Inc., Hoboken, New Jersey.
- Schrijver, C.J., Aschwanden, M.J., Title, A.M.: 2002, *Solar Phys.* **206**, 69.
- Spruit, H.C.: 1981, In Jordan, S. (ed.), *The Sun as a Star*, SP-450, NASA Washington, 385.
- Terradas, J., Oliver, R., Ballester, J.L.: 2005, *Astron. Astrophys.* **441**, 371.
- Terradas, J., Oliver, R., Ballester, J.L.: 2006, *Astrophys. J.* **650**, L91.
- Terradas, J., Andries, J., Goossens, M.: 2007, *Astron. Astrophys.*, **469**, 1135.
- Uchida, Y.: 1970, *Pub. Astron. Soc. Japan* **22**, 341.
- Van Doorselaere, T., Andries, J., Poedts, S., Goossens, M.: 2004, *Astrophys. J.* **606**, 1223.
- Verwichte, E., Foullon, C., Nakariakov, V.M.: 2006a, *Astron. Astrophys.* **446**, 1139.
- Verwichte, E., Foullon, C., Nakariakov, V.M.: 2006b, *Astron. Astrophys.* **449**, 769.
- Verwichte, E., Foullon, C., Nakariakov, V.M.: 2006c, *Astron. Astrophys.* **452**, 615.
- Zhelyazkov, I., Murawski, K., Goossens, M.: 1996, *Solar Phys.* **165**, 99.

